american physiological society
AMERICAN JOURNAL OF PHYSIOLOGY
CELL PHYSIOLOGY

Am J Physiol Cell Physiol 322: C185–C196, 2022.
First published December 8, 2021; doi:10.1152/ajpcell.00320.2021

RESEARCH ARTICLE

Notch1 and Notch3 coordinate for pericyte-induced stabilization of vasculature

Juliann B. Tefft,[1] Jennifer L. Bays,[1,2] Alex Lammers,[1,2] Sudong Kim,[1,2] Jeroen Eyckmans,[1,2] and Christopher S. Chen[1,2]

[1]*The Biological Design Center and Department of Biomedical Engineering, Boston University, Boston, Massachusetts and*
[2]*The Wyss Institute for Biologically Inspired Engineering, Harvard University, Boston, Massachusetts*

Abstract

The Notch pathway regulates complex patterning events in many species and is critical for the proper formation and function of the vasculature. Despite this importance, how the various components of the Notch pathway work in concert is still not well understood. For example, NOTCH1 stabilizes homotypic endothelial junctions, but the role of NOTCH1 in heterotypic interactions is not entirely clear. NOTCH3, on the other hand, is essential for heterotypic interactions of pericytes with the endothelium, but how NOTCH3 signaling in pericytes impacts the endothelium remains elusive. Here, we use in vitro vascular models to investigate whether pericyte-induced stabilization of the vasculature requires the cooperation of NOTCH1 and NOTCH3. We observe that both pericyte NOTCH3 and endothelial NOTCH1 are required for the stabilization of the endothelium. Loss of either NOTCH3 or NOTCH1 decreases the accumulation of VE-cadherin at endothelial adherens junctions and increases the frequency of wider, more motile junctions. We found that DLL4 was the key ligand for simulating NOTCH1 activation in endothelial cells and observed that DLL4 expression in pericytes is dependent on NOTCH3. Altogether, these data suggest that an interplay between pericyte NOTCH3 and endothelial NOTCH1 is critical for pericyte-induced vascular stabilization.

endothelium; Notch1; Notch3; pericyte; permeability

INTRODUCTION

The Notch pathway is highly conserved among species and is present in all bilateral animals (1). Notch signaling regulates diverse cell fate decisions, generating distinct patterns in many contexts. Classically, Notch receptors on "receiver" cells activate by binding Notch ligands, such as delta-like ligands (DLL) or jagged ligands (JAG), which are presented on neighboring signal "sender" cells. After binding ligand, the Notch receptor is cleaved to release a transcriptionally active Notch intracellular domain (NICD), a key effector of the Notch pathway (2–4). Active Notch transcription laterally inhibits ligand expression in these receiver cells, contributing to a feedback loop that promotes distinct boundaries and pattern formation (3).

In mammals, Notch signaling is essential for vascular function (5) and regulates angiogenesis (6), vascular development (5), and vascular barrier function (7). In endothelial cells, shear stress is one cue that activates the protein NOTCH1 (7–9) and stimulates transcriptionally independent reinforcement of vascular endothelial (VE)-cadherin at cell-cell junctions through a Rac1-mediated cortical actin assembly. In this way, active NOTCH1 reduces vascular permeability (7). NOTCH1 activation also promotes endothelial cell quiescence by upregulating connexin37 and p27 through canonical signaling (9). Interestingly, both of these mechanisms rely on the activation of NOTCH1 by presentation of the ligand DLL4 (7, 9), highlighting both the importance of Notch in homotypic cell-cell communication and the unique role of NOTCH1-DLL4 interactions compared with other Notch ligands.

In addition to homotypic cell-cell interactions, endothelial cells (ECs) engage in heterotypic interactions with mural cells. Anatomically, the endothelium is decorated externally by mural cells: pericytes (PC), which are embedded within the basement membrane of the microvasculature (10), and vascular smooth muscle cells (VSMCs), which cover larger vessels circumferentially. Functionally, pericytes have been shown to stimulate vascular barrier function and are required for blood-brain barrier development (11–13). Studies have demonstrated that several signaling pathways contribute to this heterotypic communication, such as Ang1/Tie2 (14, 15), PDGFRβ (11–13), and others (16, 17), but the potential role of Notch in communication between ECs and PCs is less clear. The NOTCH3 receptor is highly expressed in mural cells. Loss of NOTCH3 causes a marked reduction in VSMC coverage of large vessels (18–20) and arteriole hemorrhaging in mice (18), but the precise role of NOTCH3 in pericytes is less clear. Conflicting reports suggest that loss of NOTCH3 does not impact pericyte localization and distribution (18), whereas others have described progressive loss of pericytes (20). NOTCH3 phenotypes impact small vessels where pericytes predominate, mutations in NOTCH3 cause the vascular disease CADASIL (cerebral autosomal dominant arteriopathy with subcortical infarcts and leukoencephalopathy) (21), and NOTCH3 SNPs have been linked to age-related small vessel disease (SVD) (22). CADASIL and SVD progressively

Correspondence: C. S. Chen (chencs@bu.edu).
Submitted 30 August 2021 / Revised 24 November 2021 / Accepted 7 December 2021

increase the risk of dementia and stroke (23), suggesting a role for NOTCH3 in small vessel homeostasis and raising the question of how Notch signaling contributes to heterotypic communication in the microvasculature.

Here, we sought to investigate whether pericytes stabilize endothelium by engaging in endothelial NOTCH1 signaling and whether loss of NOTCH3 signaling in pericytes interrupts this stabilizing interaction. We used in vitro microvessel models to systematically evaluate how NOTCH3 in pericytes and NOTCH1 in endothelial cells contribute to the formation of stable vascular junctions. We found that pericytes stabilize vascular cell junctions in vitro; however, loss of either pericyte NOTCH3 or endothelial NOTCH1 prevents this stabilization from occurring. We observed that DLL4 is the critical ligand for activating NOTCH1 in endothelial cells and show that DLL4, but not JAG1, stimulates vascular barrier enhancement. Furthermore, we observe that pericytes upregulate DLL4 in response to JAG1 binding in a NOTCH3-dependent manner. Altogether, we suggest a previously unappreciated interplay between NOTCH1 and NOTCH3 that coordinates pericyte-induced vascular stability.

MATERIALS AND METHODS

Cell Culture

Human neonatal dermal blood microvascular endothelial cells (HMVEC-dBlNeo, Lonza) were cultured in endothelial microvascular cell growth medium (EGM2-MV, Lonza) and used before *passage 7*. Human brain vascular pericytes (HBVPC, ScienCell) were cultured in pericyte medium (PM, ScienCell) and used before *passage 7*. Human aortic smooth muscle cells (hASMC, Lonza) were cultured in smooth muscle medium (SMCM, ScienCell). Medium for all cell types was replaced every 2 days between passages. All cells were cultured in a humidified incubator at 37°C with 5% CO_2.

Lentiviral Transduction and CRISPR Knockout Lines

Stable CRISPR knockout lines in the HBVPCs were generated using the lentiCRISPRv2 system (from F. Zhang, Addgene plasmid #52961). The guide RNA sequences used for silencing were generated using CRISPOR (24) and are listed in Supplemental Table 1 (all Supplemental Tables and Figures are available at https://doi.org/10.6084/m9.figshare.16499511.v1). Guides were cloned into the lentiCRISPRv2 plasmid at the BsmbI site. Lentivirus was produced by cotransfecting HEK 293 T cells with each individual lentiviral plasmid and with the pVSVG, pRSV-REV, and pMDLg/pRRE packaging plasmids using a calcium phosphate transfection method. Virus-containing supernatant was collected 48 h after transfection, concentrated using PEG-it Virus Precipitation Solution (SBI), resuspended in Optimem (Gibco) and flash frozen at −80°C. HBVPCs were infected with the CRISPR lentivirus in growth medium for 16–20 h, then cultured in normal growth medium until confluent. Once confluent, 2 μg/mL of puromycin was added to normal growth medium for 2–3 days to select for mutant cells. Western blots were used to verify knockout efficiency.

Device Fabrication

The three-dimensional (3-D) microvessel chip has been previously published (25). In short, polydimethylsiloxane (PDMS, Sylgard 184, Dow-Corning) was mixed at a standard ratio of 1:10 (w/w) of PDMS base to crosslinking reagent. This mixture was poured over a silicon master wafer with positive relief structures of photoresist (SU-8, microchem), degassed in a vacuum chamber until bubbles dissipated, and cured for 2 h on a hot plate set to 80°C. This PDMS was removed from the mold and cut into individual devices. A 1.5-mm biopsy punch was used to form the sites for gel injection and 6-mm biopsy punch was used to make media reservoirs. The PDMS devices were then bonded to cover glass (VWR International, LLC) by activation of the surface via plasma treatment for 30 s. Bonded devices were incubated in a 100°C oven overnight. Devices were sterilized before use by 15 min of UV light exposure.

Formation of Microvessel Networks

HMVECs and HBVPCs were lifted from the tissue culture plates with 0.05% Trypsin-EDTA and centrifuged at 200 *g* for 4 min. HMVECs were resuspended in EGM2-MV at 6.6 million cells/mL, and HBVPCs were resuspended at 8 million cells/mL. A fibrinogen solution of 12 mg/mL (Fibrinogen from Bovine Plasma, Sigma) was prepared by resuspending the fibrinogen in D-PBS with calcium and magnesium (Thermo Fisher Scientific) and was filtered through a 0.2-μm filter before use. The lateral gel regions were not seeded with cells in these experiments, and so 2.5 mg/mL fibrinogen + 0.16 U/mL aprotinin (Sigma) were mixed with 1 U/mL of thrombin (Sigma) and injected into the lateral channels before cell seeding. A master mix was prepared with final concentrations of HMVECs at 4 million cells/mL, fibrinogen at 2.5 mg/mL, human fibronectin (Corning) at 10 μg/mL, and aprotinin at 0.16 U/mL. Devices containing pericytes included a final concentration of HBVPCs at 0.8 million cells/mL in the master mix as well. Master mix (35 μL) was mixed with thrombin at 1 U/mL and rapidly injected into the central channels of three devices in succession. After polymerization of the fibrin gel, EGM2-MV media was added to the reservoirs and pulled into the media channels using vacuum application. Fresh EGM2-MV containing additional 12.5 ng/mL VEGF-A and 12.5 ng/mL b-FGF was added to the four media reservoirs and was replaced after 48 h. Devices were cultured on a level surface in a humidified incubator at 37°C with 5% CO_2. Every 12 h, 15 μL of media was moved from the right to left media reservoir to induce a 30 μL pressure gradient of flow across the central gel region. All devices were fixed on *day 3* or *4*.

Antibodies and Reagents

Antibodies against VE-Cadherin (Ms, F-8: sc-9989, 1:1,000 IF, 1:5,000 WB) and Jagged-1 (Ms, sc-390177, 1:500 WB) were from Santa Cruz Biotechnology. Antibodies against total Notch1 (Rb, D1E11, 1:5,000 WB), cleaved Notch1-Val1744 (Rb, 4147, 1:500 WB), GAPDH (Rb, 2118, 1:10,000 WB), β-actin (Ms, 3700, 1:10,000 WB), anti-mouse IgG HRP-linked antibody (7076, 1:10,000 WB), and anti-rabbit IgG HRP-linked antibody (7074, 1:10,000 WB) were from Cell Signaling Technology. Antibodies against Dll4 (Rb, ab7280, 1:1,000 WB) and NG2 (Rb, ab275024, 1:1,000 IF) were from Abcam. Rhodamine and Alexa Fluor 488-labelled phalloidin and Alexa Fluor Plus 488, 568, and 647 goat anti-mouse and anti-

rabbit IgG highly cross-adsorbed secondary antibodies were from Life Technologies. Phalloidins were used at 1:100 dilution and secondary antibodies for immunofluorescence were used at a 1:1,000 dilution. DAPI and DAPT (D5942) were from Sigma. UEA Lectin (UEA DyLight 649, DL-1068, 1:200) was from Vector Labs. Recombinant human DLL4 Fc Chimera protein (10185-D4), recombinant human JAG1 Fc Chimera protein (1277-JG), recombinant human NOTCH3 (AA 40–467) Fc chimera protein (1559-NT), recombinant human IgG Fc (110-HG), and recombinant human VEGF-A (293-VE) were from R&D systems. Recombinant human b-FGF (PHG0261) was from Thermo Fisher Scientific. Reagents for siRNA transfection were purchased from Horizon Discovery, including Dharmafect 1 Transfection Reagent (T-2001), ON-TARGETplus Human NOTCH1 SMARTpool siRNA (L-007771-00-0010), and ON-TARGETplus Non-targeting Control Pool (D-001810-10-05).

Immunofluorescence

Vascular networks were fixed at 37°C for 15 min using warm 4% paraformaldehyde diluted in PBS containing calcium and magnesium (PBS++). All staining solutions were diluted in PBS++ and rinses were performed with sterile PBS++. Samples were rinsed with three times after fixation then permeabilized with 0.2% triton-X-100 for 15 min at room temperature. Samples were then blocked in 3% bovine serum albumin (Sigma) for 3 h at room temperature. Primary and secondary antibodies were added into cold blocking solution and stained overnight at 4°C using 50 μL of pressure-driven flow across the central channel. Antibodies were rinsed by pressure-driven flow at room temperature.

Imaging

Fluorescent images were captured on a Leica SP8 confocal microscope (Leica, Wetzlar, Germany) using either a Leica ×10/0.30 NA or ×25/0.95 NA water objective and the Leica LAS X imaging software. Identical laser intensities and microscope settings were held constant across all samples for each experiment.

Quantification of Vascular Area Coverage

To quantify the area covered by vasculature in the microvessel devices, ×10 images through the full depth of the vasculature were captured. In ImageJ (26), the 3-D image stack was reduced to 2-D with a max projection. This projected image was "smoothed" and "despeckled" to reduce noise then a manual threshold was used to generate a binary image of the vasculature. The percentage of nonzero area for each image was measured and reported as the percentage of area covered by vasculature. Vascular area was quantified across three independent experiments and quantified from two to three technical replicates per experiment.

Junctional Width Quantification

To prevent fluorescent image bleed through between junctional stains, vessels were stained and imaged with p120-catenin in green (488 nm) and VE-cadherin at far red (647 nm). Maximum *z*-projections of confocal images at ×25 magnification were compiled to isolate single sides of a vessel using ImageJ (26). These images were then separated for each color channel and identical lines were drawn perpendicular to a single junction on both the p120 and VE channel image. These lines were quantified using the "plot profile" command then the data points were combined onto a single plot, and the data were extracted and saved in a comma-separated values (.csv) file. These data were exported into MATLAB, where a script was applied to fit a polynomial to the data set and the width of the junction at ¼ of maximum height was measured and recorded. The polynomial and original data points were overlaid on a plot to verify an accurate fit, and the fit parameters were adjusted to correct poor fits as needed. Data were gathered across three independent experiments. For each experiment, 1–2 confocal images were collected from each of the 3 technical replicates, and 12–20 junctions measured per image.

Junctional Intensity Quantification

The intensity of VE-cadherin and p120-catenin at cell junctions was obtained from maximum *z*-projections of confocal images. A consistent threshold was applied to all images per experimental batch to remove background signal. The total fluorescent signal intensity per channel was then quantified and normalized to the junctional area, yielding an average intensity per pixel. Data were gathered across three independent experiments. For each experiment, one to two confocal images were collected from each of the three technical replicates. To compare between experiments, intensity per pixel values were normalized to the maximum value per experiment, yielding a range of intensities from 0 to 1.

Quantitative Polymerase Chain Reaction

Pericytes were lysed in Trizol (Life Technologies). To purify RNA, the aqueous phase was isolated with phenol-chloroform extraction, mixed 1:1 with 70% ethanol, loaded onto an RNA micro column (Qiagen), and recovered by following the kit protocol. Isolated RNA (800 ng) was converted to cDNA with qScript cDNA Supermix (QuantaBio). Real-time PCR was performed with Power SYBR Green Master Mix (Thermo Fisher Scientific) on an Applied Biosystems QuantStudio three Real-Time PCR System (Thermo Fisher Scientific). Specific primers used for qPCR are listed in Supplemental Table 2.

siRNA Transfection

Endothelial cells were plated into a 6-well plate in antibiotic-free EGM2-MV 24 h before siRNA transfection. Transfection reagents and siRNA were diluted in Optimem and added to the well of 80% confluent cells, according to manufacturer instructions. For HMVECs, 2 μL of transfection reagent was used per well, and siRNA were added for a final concentration of 40 nM. After 24 h, cells were lifted and used in downstream experiments. Cells were lysed for Western blot at 96 h posttransfection to quantify knockdown. This timepoint coincided with the end point of the 3-D microvessel experiments.

Cell Lysis and Western Blot

All cells were lysed in RIPA buffer + 2X protease & phosphatase inhibitors (Thermo Fisher Scientific, 78442), homogenized 3X through a 25-g needle, spun at 15,000 *g* for 15 min.

Protein content was quantified using the Pierce BCA protein assay kit (Thermo Fisher Scientific, 23225). The supernatant was then diluted with LDS loading buffer (Thermo Fisher Scientific, NP0007), β-mercaptoethanol was added to a final 5% concentration, and samples were boiled at 100°C for 5 min. Samples were frozen at −20°C until analysis by Western blot. For western blots, protein loading was normalized by protein content across wells. NuPAGE Bis-Tris gels (Thermo Fisher Scientific) were run at 180 V in MOPS buffer (Thermo Fisher Scientific) then gels were blotted onto a PDVF membrane in NuPAGE transfer buffer (Thermo Fisher Scientific) at 125 mA for 2 h. Blots were blocked in TBST + 5% milk for 1 h then primary antibodies were added in milk overnight on a rocker. After rinsing 3X at room temperature, secondaries were applied at 1:5,000 for 1 h, rinsed 3X, developed for 4 min with SuperSignal West Dura Extended Duration Substrate (Thermo Fisher Scientific), and imaged on an iBright Imaging System (Thermo Fisher Scientific) using the automatic exposure option. Western blots were quantified by integrated density using ImageJ (26), normalized for background, and normalized to a loading control per sample. All Western blot samples were gathered across three independent experiments and quantification represents these independent samples.

Recombinant Ligand Coatings

For all coating experiments, proteins were diluted in PBS to final concentrations of 0.4 μg/mL for IgG1, 1 μg/mL for rDLL4, 2 μg/mL for rJAG1, and 1 μg/mL for rN3-ECD. These protein concentrations were chosen to normalize for the molecular weight (MW) of each protein of interest. For 2-D Western blot experiments, 1 mL of diluted ligand was added to a tissue culture treated 6-well plate at 37°C for 2 h to coat. Wells were then rinsed before plating cells onto the coated surfaces. Pericytes were plated onto these coated wells at 100,000 cells/well, ECs were plated at either a low density of 75,000 cells/well (Fig. 5*A* and Supplemental Fig. S4) or a high density of 310,000 cells/well (Supplemental Fig. S4). Cells were lysed after 24 h. For low density wells, 3-wells were pooled together per condition. For ligand-coated human-engineered microvessel (hEMV) channels, 100 μL of ligand containing PBS was added into the reservoirs, and the devices were incubated on a rocker overnight. Channels were rinsed before introducing HMVECs, and permeability was measured after 24 h.

hEMV and Permeability

The method for preparing the single microvessel device has been previously described in great detail (27). Vessels containing pericytes were formed by seeding pericytes at a 1:5 ratio to endothelial cells. The pericytes were introduced into the channel first and allowed to adhere for 1 h before seeding the endothelial cells. hEMV devices were cultured on a rocking platform in the incubator to introduce oscillatory flow through the channels until permeability was measured.

The method for measuring the permeability of vessels has been previously described by our laboratory in great detail (27). After 24 h of seeding, hEMV devices were removed from the rocker and placed on a static incubator shelf for 1 h. Permeability was measured using 70 kDa Texas Red conjugated dextran (Thermo fisher Scientific). Samples were imaged on a Yokogawa CSU-21-Zeiss Axiovert 200 M inverted spinning-disk microscope using a Zeiss ×10 air objective and an Evolve EMCCD camera (Photometrics). Images were captured every 5 s for 2 min, and permeability coefficients were calculated using MATLAB image analysis.

RESULTS

Microvessel Model for Studying the Effect of Pericytes on Developing Vasculature

We used a 3-D in vitro microvessel model to investigate the impact of pericytes on developing vasculature. For this model, human microvascular endothelial cells (ECs) and human brain vascular pericytes (PCs) were mixed into a solution composed of 2.5 mg/mL fibrinogen and 10 μg/mL fibronectin, then injected into a PDMS mold where it polymerized to form a gel in the mold. This model has been previously been utilized for the formation of rapid and robust vascular networks (25). After 3 days, vascular networks were formed both with and without pericytes present, but coculture with pericytes resulted in significant condensation and narrowing of the conduits within the vascular network (Fig. 1*A*), consistent with prior observations (28, 29). Two-dimensional projections of the 3-D vascular structures were used to quantify the approximate area covered by the vasculature. This vascular area decreased from 67.3 ± 3.6% with endothelial cells alone to 44.0 ± 9.6% in vasculature cocultured with pericytes. To document cellular distribution in these networks, we observed that NG2-expressing pericytes were associated with lectin positive endothelium (Fig. 1, *B* and *C*), indicating that pericytes did localize to the endothelium within these vascular networks. Cross-sectional images at higher magnification revealed an association of the NG2 + pericytes with the vasculature. Line sampling of the intensity within the XY imaging plane revealed a phalloidin signature at the borders of both the UEA lectin-stained endothelium and the NG2 + pericytes (Fig. 1*C*).

Pericytes Maintain Their Identity and Support Vasculogenesis without NOTCH3

To investigate the role of NOTCH3 in these pericytes, we generated pericytes harboring stable CRISPR-Cas9-mediated *NOTCH3* gene knockout ($N3^{KO}$) and nontargeting control (Scr) pericytes. Despite the knockout strategy, the mutant $N3^{KO}$ cell population used in this study still expressed 11 ± 4.1% of NOTCH3 protein compared with Scr controls (Fig. 2*A*). Given the importance of NOTCH3 for mural cell differentiation (19, 20, 30, 31), we sought to verify that the absence of NOTCH3 had not caused a phenotype change in these cells by using qPCR to assess whether NOTCH3 loss impacted the expression of key pericyte markers. The interaction of pericyte NOTCH3 and endothelial JAG1 has been shown to be essential for pericyte recruitment and differentiation (30, 32); therefore, we assessed the pericytes in three different Notch activation states, a neutral state, plated on a recombinant IgG1 control protein, an active state, plated on rJAG1 protein, or an inactive state, plated on rJAG1 with γ-secretase inhibitor DAPT added to the media. After 12 h of plating, we

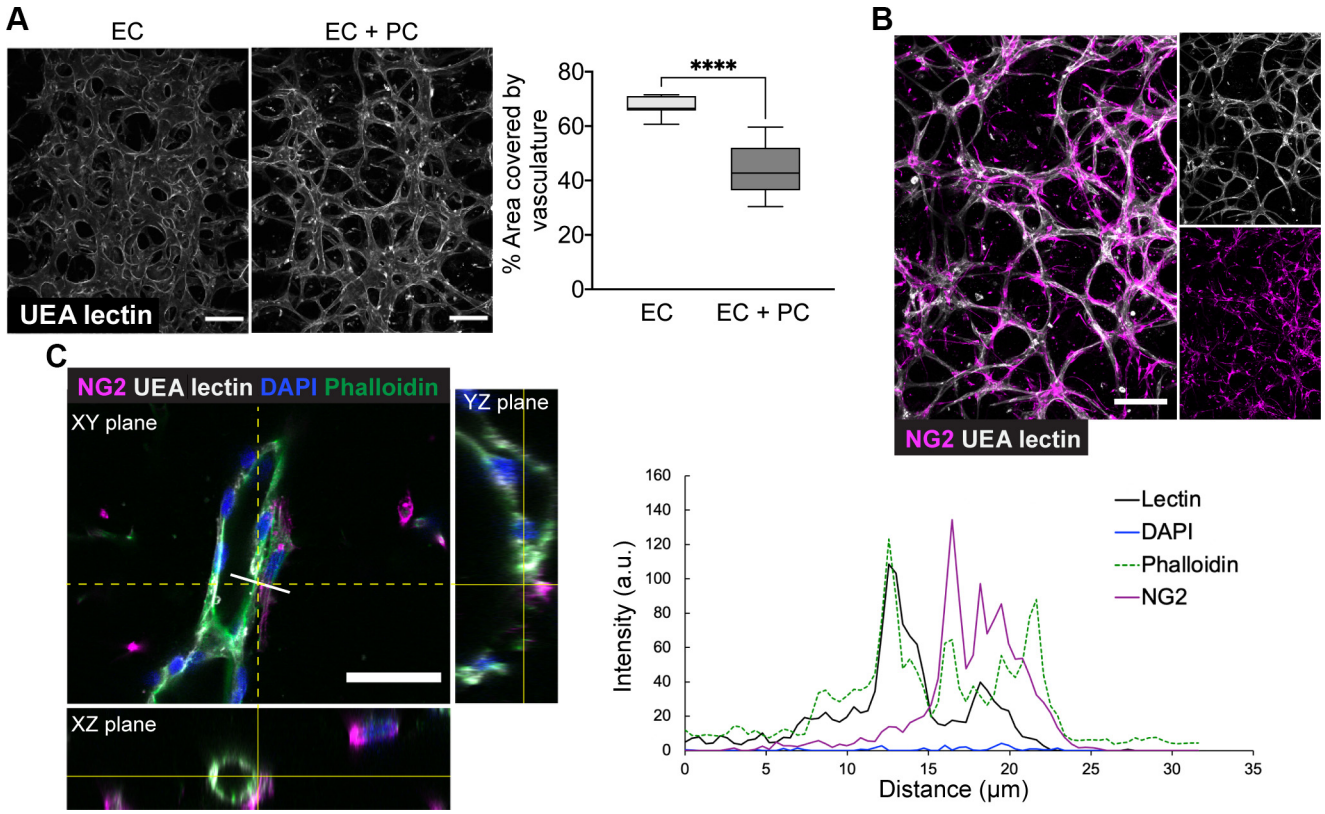

Figure 1. Pericytes support vasculogenesis. *A*: UEA lectin-stained vasculature after 3 days of coculture with human brain vascular pericytes (*left*), and quantification of the vascular area (*right*). Box plot with whiskers calculated using Tukey's method. *P* values calculated with two-tailed unpaired Student's *t* test. ****$P < 0.0001$. Scale bar 150 μm. *B*: ×10 images of vasculature showing NG2$^+$ pericytes (magenta) overlaid with UEA lectin (gray) endothelium. Scale bar 150 μm. C: cross-sectional views of a vessel and associated pericyte. Yellow dotted lines indicate the locations for the corresponding YZ and XZ planes. The white line indicates the location where a line scan was used to generate the corresponding intensity profiles (*right*). Scale bar 50 μm.

observed robust activation of the Notch downstream genes *HEY1, HES1,* and *HES6* in our Scr PC, whereas only *HES1* expression was maintained in the N3^{KO} PC. Inhibition of γ-secretase with DAPT abrogated the upregulation of *HEY1* and *HES1*. Interestingly, *HES6* expression was robustly increased on JAG1 in a NOTCH3-dependent manner, but *HES6* expression was not blocked by the addition of DAPT (Fig. 2*B*). Next, we investigated whether N3^{KO} would impact the expression of pericyte markers in these cells. The N3^{KO} pericytes robustly expressed pericyte markers, including *NG2, RGS5, PDGFRB,* and *CDH2* among others and this expression did not appear to change with Notch signaling, with no significant differences of −ΔCt values between Scr and N3^{KO} pericytes (Fig. 2*C*). In addition, there were no significant differences between Notch-activated or Notch-inhibited conditions, indicating that NOTCH3 knockout did not cause a loss of pericyte identity.

We then examined the effect of these cells in the in vitro vascular network formation assay. Representative images of the resulting vessels (Fig. 2*D*) depict UEA lectin-stained endothelium and endothelial nuclei stained with the transcription factor ERG. Although this condensation was reduced in comparison with vasculature cocultured with wild-type (WT) pericytes, vessels formed with the Scr and N3^{KO} pericytes condensed the vasculature to the same extent (Fig. 2*E*), suggesting some background effect of the CRISPR system. Nonetheless, loss of NOTCH3 did not significantly alter the architecture of the vasculature compared with vessel networks formed with Scr PC. Of note, the endothelial cells used in these experiments do not express NOTCH3, whereas both the endothelial cells and pericytes express NOTCH1 (Supplemental Fig. S1).

Pericyte-Induced Stabilization of the Endothelium Requires Pericyte NOTCH3

Although the macrostructure of the vessels cocultured with pericytes was not significantly altered by N3^{KO}, we did observe a difference in the junctional morphology of vessels formed with Scr versus N3^{KO} pericytes. Staining for VE-cadherin, the primary adherens junction molecule in endothelial cells (33), and for p120-catenin, a multifaceted scaffolding protein that binds VE-cadherin to prevent cadherin endocytosis (34, 35), revealed differences in the intensity and width of junctions in the N3^{KO} vasculature (Fig. 3). Quantification of the intensity and distribution of VE-cadherin and p120-catenin at the cell junctions showed that vessels cocultured with Scr PCs had significantly increased VE-cadherin intensity at junctions compared with vessels formed with endothelial cells alone or with N3^{KO} pericytes (Fig 3*Bii*), and that intensity was distributed more tightly to form a well-delineated, thin, linear cell-cell interface (Fig 3*Biii*). In contrast, vessels formed with N3^{KO} pericytes

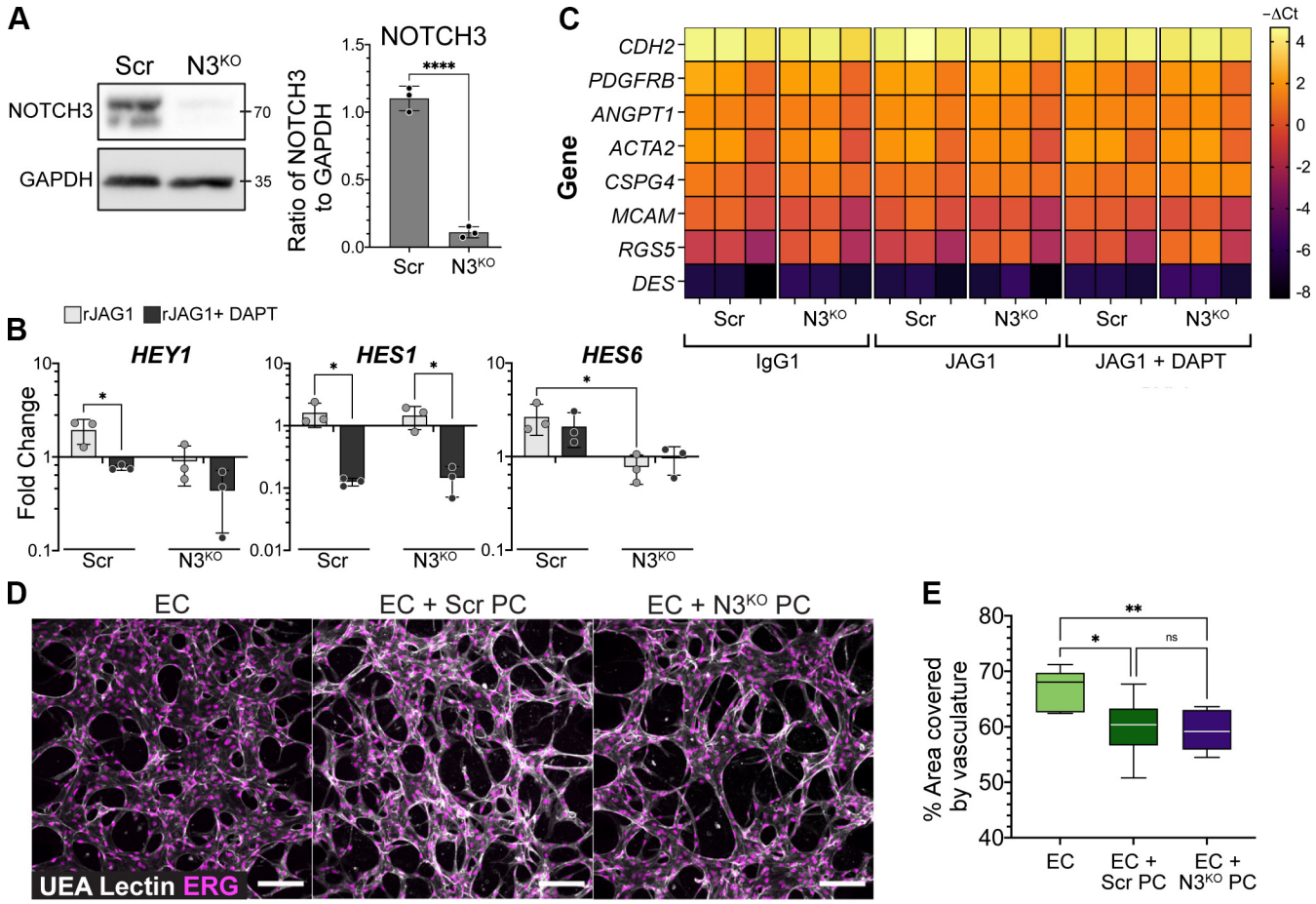

Figure 2. Pericytes maintain their identity and support vasculogenesis without NOTCH3. *A*: Western blot of NOTCH3 expression in Scr and N3^{KO} pericytes (*left*) and quantification of NOTCH3 content in both cell types, normalized to loading control (*right*). Means ± SD. *P* values calculated with two-tailed unpaired Student's *t* test, ****$P < 0.0001$. *B*: fold change in gene expression 12 h after plating the pericytes on surfaces coated with either rIgG1, rJAG1, or rJAG1 with DAPT. Fold change is relative to IgG1 condition and GAPDH. *P* values calculated with ordinary two-way ANOVA with multiple comparisons. *$P < 0.05$. *C*: heat map depicting qPCR −ΔCt values for pericyte genes relative to GAPDH housekeeping gene. Scr and N3^{KO} pericytes were plated in three different Notch states (on IgG1: neutral, on JAG1: active, on JAG1 + DAPT: inactive) for 24 h before lysis. *C*: representative images of vascular networks formed with endothelial cells alone, in coculture with Scr pericytes and in coculture with N3^{KO} pericytes. Scale bar 150 μm. *D*: quantification of vascular area coverage in the three different culture conditions from *C*. *E*: box plot with whiskers calculated using Tukey's method. *P* values calculated with ordinary one-way ANOVA with multiple comparisons. *$P < 0.05$, **$P < 0.01$.

showed no significant increase in VE-cadherin intensity compared with the vessels formed with endothelial cells alone, and the distribution of intensity across junctions suggested more broad and jagged cell-cell interface that has previously been associated with less stable junctions (36). The intensity of p120-catenin at the cell junctions showed a similar trend, except that coculture with N3^{KO} pericytes also showed a statistically significant increase in p120 intensity, though not to the same extent as Scr PCs (Fig. 3*C*). All samples were treated identically through the fixing, staining, and imaging process, therefore, normalized intensity differences between samples were considered to be representative of biochemical changes in protein accumulation, an approach that has been effectively used previously (37, 38). Together, these results indicate that NOTCH3 contributes to the stabilization of endothelial junctions, and loss of NOTCH3 reduces pericyte-induced stabilization of the endothelium.

To verify that our junctional observation was representative of a physiological difference in vascular barrier, we used a human engineered microvessel (hEMV) that was previously been developed by our laboratory (7, 27, 39) to measure permeability on vessels formed with and without pericytes. Consistent with our junctional width and intensity observations, we observed that vessels cultured with endothelial cells alone were highly permeable, whereas the vessels cocultured with pericytes showed a reduced permeability. Interestingly, we observed a significant decrease in vascular permeability with both Scr and N3^{KO} pericytes but the N3^{KO} pericytes had a significantly reduced capacity to stabilize the vascular barrier (Fig. 3*D*, Supplemental Movie 1; see https://doi.org/10.6084/m9.figshare.16499517.v1).

Pericyte-Induced Stabilization of the Endothelium Requires Endothelial NOTCH1

Next, we investigated the role of endothelial cell NOTCH1 on the developing vasculature with and without pericytes. Prior work has shown that activation of NOTCH1 within endothelial cells enhances vascular junction stabilization (7, 8),

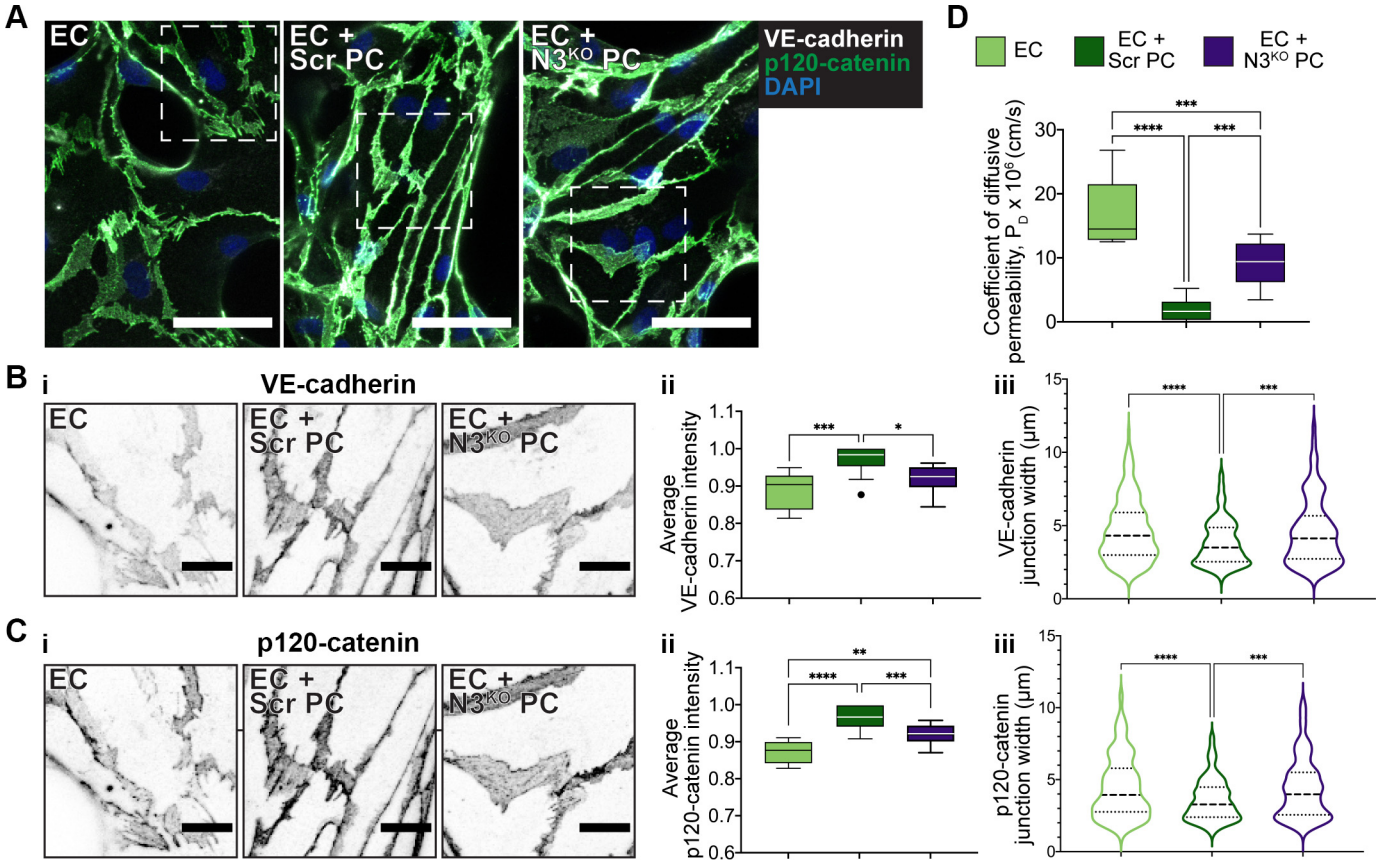

Figure 3. Pericyte-induced stabilization of the endothelium requires NOTCH3. *A*: representative images of endothelial junctions in vascular networks formed with endothelial cells alone, in coculture with Scr pericytes, or in coculture with N3^{KO} pericytes. VE-cadherin in white, p120-catenin in green, and DAPI in blue. Scale bar 50 μm. *B*: *i*) Higher magnification inset of VE-cadherin staining. Scale bar 15 μm. *ii*) Quantification of junctional VE-cadherin intensity. *iii*) Quantification of junctional widths for VE-cadherin. *C*: *i*) higher magnification inset of p120-catenin staining. Scale bar 15 μm. *ii*) Quantification of junctional p120-catenin intensity. *iii*) Quantification of junctional widths for p120-catenin. For *Biii* and *Ciii*, outliers were removed with ROUT test with Q of 1%. *D*: quantification of the coefficient of diffusive permeability of 70 kDa dextran for hEMV seeded with endothelial cells (ECs) alone, ECs with Scr PC, or ECs with N3^{KO} PC. For *Bii*, *Cii*, and *D*, whiskers were calculated using Tukey's method. For all, *P* values calculated using ordinary one-way ANOVA with multiple comparisons. $*P < 0.05$, $**P < 0.01$, $***P < 0.001$, $****P < 0.0001$.

but that the presence of inactive NOTCH1, such as in conditions where the γ-secretase inhibitor DAPT is used to inhibit cleavage of the NOTCH1 intracellular domain is not sufficient to stabilize junctions (7). Therefore, we hypothesized that pericytes could be directly activating NOTCH1 within the endothelium to stabilize vascular junctions. To test this, we treated endothelial cells with either nontargeting siRNA control (siCtrl) or siRNA targeting *NOTCH1* (siN1) to see whether the loss of endothelial NOTCH1 impacted the ability for pericytes to enhance vascular junctions. For this experiment, we chose to use siRNA instead of CRISPR-guided *NOTCH1* knockout to avoid the severe defects in endothelial cells caused by complete NOTCH1 loss of function (7). Endothelial cells were transfected with siRNA for 24 h before seeding devices, and the vessels were fixed at 96 h posttransfection, at which point remaining siRNA-treated ECs were lysed and verified for knock down. The relative amount of NOTCH1 protein in the siN1 ECs at this timepoint was 63.1 ± 11% (Supplemental Fig. S2). In coculture, pericytes condensed the vasculature to largely the same extent regardless of the NOTCH1 expression state of the endothelial cells (Supplemental Fig. S3). However, staining for VE-cadherin and p120-catenin revealed a decreased capacity for the pericytes to stabilize junctions in ECs depleted of NOTCH1 (Fig. 4). Representative images of the staining of these vessels are shown in Fig. 4*A*. Quantification of the intensity and distribution of VE-cadherin and p120-catenin at the cell-cell junctions of siCtrl ECs cocultured with pericytes as with wild-type ECs demonstrated a significant increase in staining intensity and linearity of both VE-cadherin and p120-catenin. In contrast, for the siN1 ECs, there was no significant increase in VE-cadherin staining intensity upon PC coculture with a more jagged junctional distribution of staining across junctions (Fig. 4*B, ii* and *iii*), there was, however, a significant increase of p120-catenin intensity but the junctional distribution remained jagged and less linear (Fig. 4*C, ii* and *iii*). These data indicate that the pericytes need endothelial NOTCH1 to stabilize the endothelial cell junctions.

DLL4 Stimulates NOTCH1 Activation and Barrier Enhancement

We next sought to verify whether vascular junction reinforcement relied on signaling from a specific Notch ligand. Based on our results, we considered two possible hypotheses to explain how pericytes might activate NOTCH1 in the

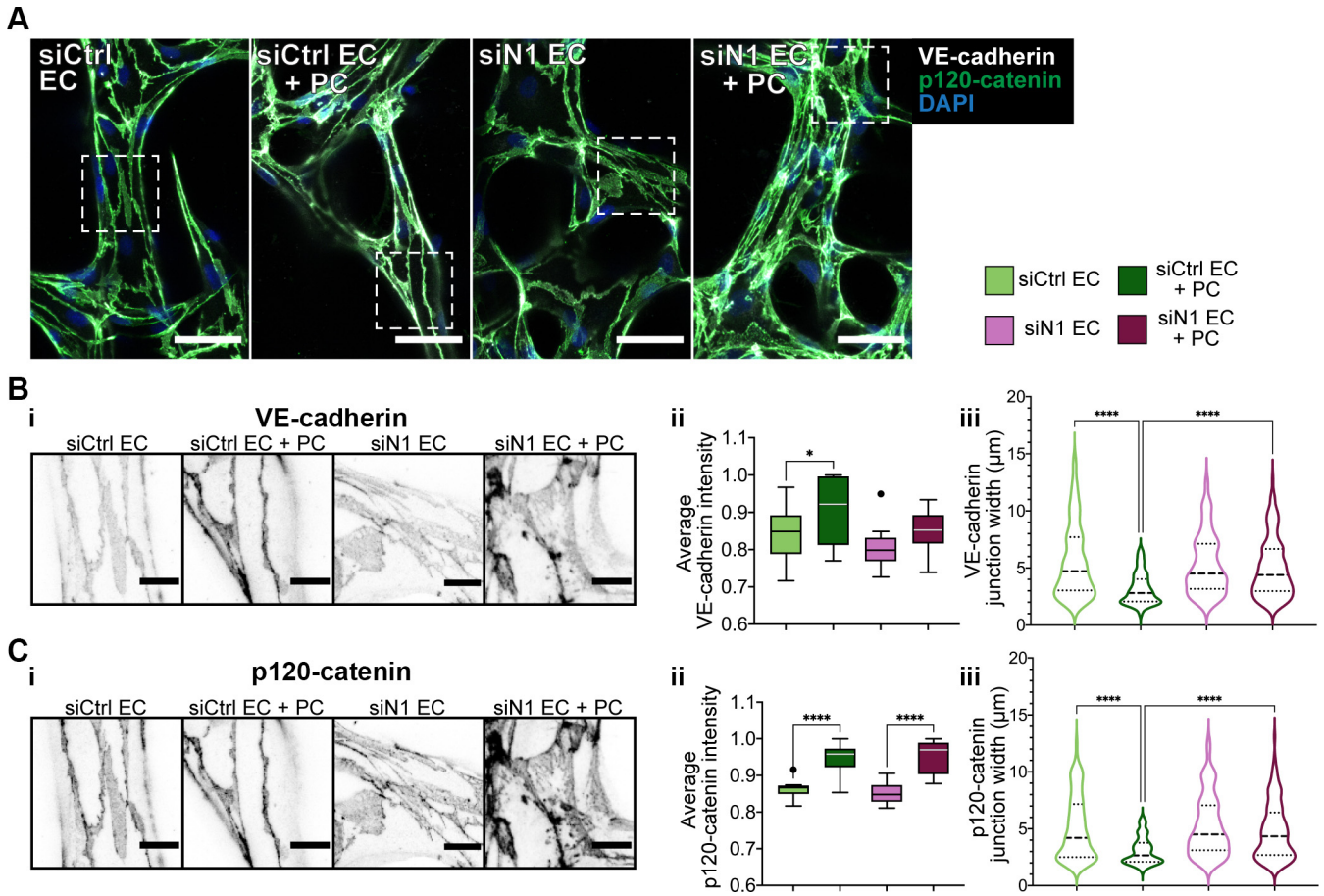

Figure 4. Pericyte-induced stabilization of the endothelium requires NOTCH1. *A*: representative images of endothelial junctions in vascular networks formed with siCtrl of siN1 endothelial cells alone, or in coculture with pericytes. Overlay with VE-cadherin in gray, p120-catenin in green, and DAPI in blue. Scale bar 50 μm. *B*: *i*) higher magnification inset of VE-cadherin staining. Scale bar 15 μm. *ii*) Quantification of junctional VE-cadherin intensity. *iii*) Quantification of junctional widths for VE-cadherin. *C*: *i*) Higher magnification inset of p120-catenin staining. Scale bar 15 μm. *ii*) Quantification of junctional p120-catenin intensity. *iii*) Quantification of junctional widths for p120-catenin. For *Biii* and *Ciii*, outliers were removed with ROUT test with Q of 1%. For *Bii* and *Cii*, whiskers were calculated using Tukey's method. For all, *P* values calculated using ordinary one-way ANOVA with multiple comparisons. $*P < 0.05$, $**P < 0.01$, $***P < 0.001$, $****P < 0.0001$.

endothelial cells. First, DLL4 expressed by pericytes could directly bind to EC NOTCH1, causing receptor activation. Second, it is possible that NOTCH3 could indirectly alter the ligands dominating the junctions between endothelial cells. If pericyte NOTCH3 preferentially binds the JAG1 expressed by endothelial cells, this could sequester JAG1 from endothelial-endothelial NOTCH1 engagement, leaving a higher proportion of NOTCH1 available to bind DLL4 between endothelial cells. To test these possibilities, we examined the effects of seeding cells onto tissue culture plates coated with recombinant DLL4, JAG1, NOTCH3 extracellular domain (rN3ECD), or an IgG1 control. For rDLL4 and rJAG1, we plated endothelial cells on top of these coated surfaces at low density to minimize cell-cell contacts and maximize binding with the coated ligand (Fig. 5*A*). For rN3ECD, we tested both a low-density and confluent layer of endothelial cells on the coated surfaces in case cell-cell contacts were required for the sequestration mechanism to occur (Supplemental Fig. S4). In all conditions, endothelial cells were lysed after 24 h and assessed for alterations in NOTCH1 activation. For the endothelial cells on rN3ECD, we did not observe significant changes in NOTCH1 activation at either density (Supplemental Fig. S4), suggesting that sequestration of JAG1 by N3ECD was not sufficient to activate endothelial NOTCH1. Endothelial cells plated on rDLL4, however, increased NOTCH1 cleavage (Val1744) compared with cells plated in IgG1, whereas cells plated on rJAG1 showed an insignificant increase of NOTCH1 cleavage (Fig. 5*A*). These data corroborate prior observations that DLL4 is the key ligand that activates NOTCH1 in endothelial cells.

We next sought to verify that DLL4 was also stimulating a functional change in vascular barrier function using the hEMV permeability assay. Here, we coated the collagen channels with recombinant protein, seeded endothelial cells into these channels, and measured the permeability 24 h later. We found that rDLL4 coating improved vascular barrier function and reduced the coefficient of diffusive permeability, whereas rJAG1 coating did not significantly reduce vascular leak compared with the IgG1 control (Fig. 5*B*, Supplemental Movie 2; see https://doi.org/10.6084/m9.figshare.16499547.v1). These data suggest that DLL4 is a key ligand for inducing NOTCH1-mediated changes in endothelial cell-cell junctions.

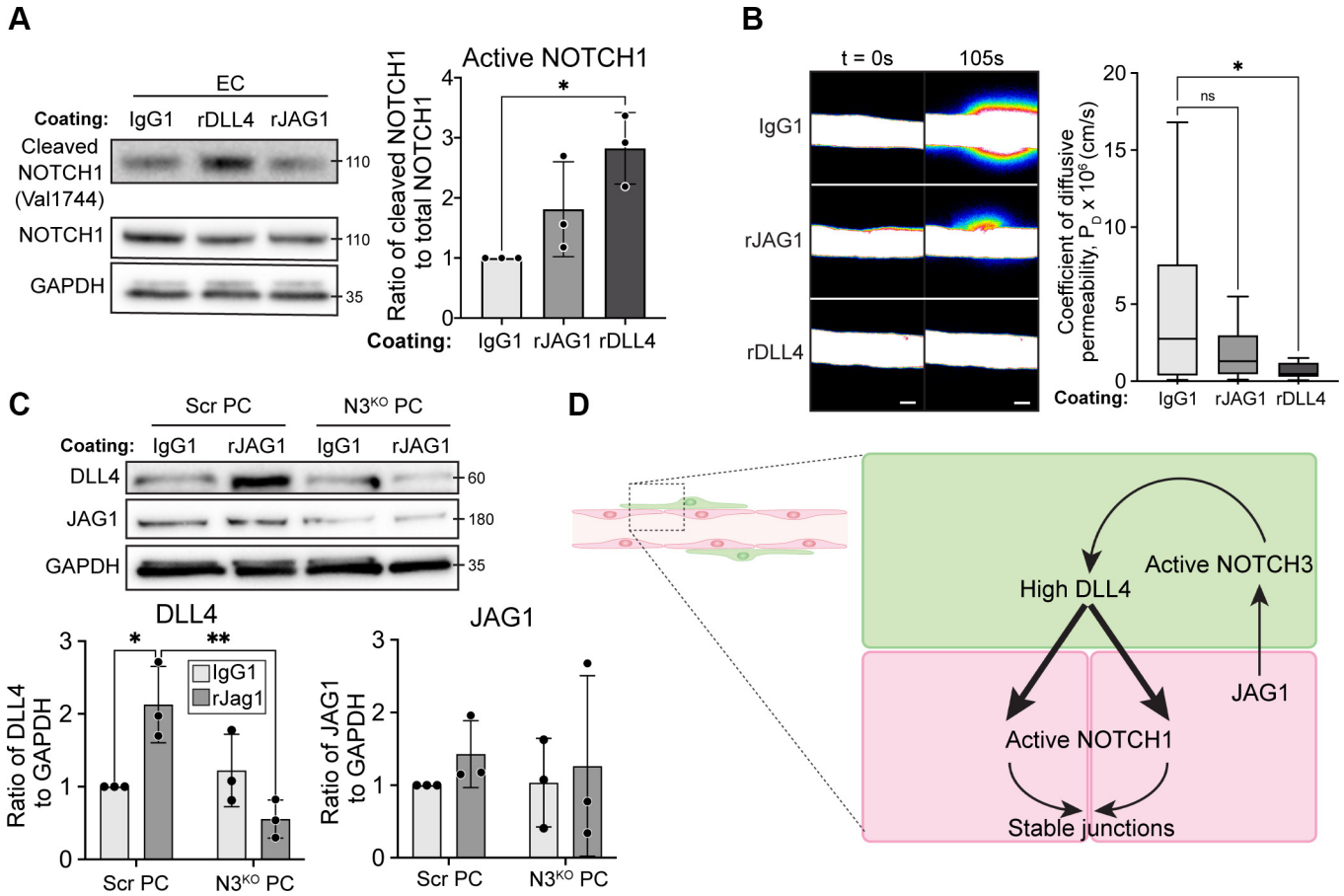

Figure 5. Pericytes upregulate DLL4 in a Notch-dependent manner to stabilize the endothelium. *A*: Western blot of endothelial cells (ECs) plated on plates coated with recombinant IgG1, rJAG1, or rDLL4 (*left*) and quantification of the ratio of active (cleaved) NOTCH1 to total NOTCH1 in each condition (*right*). Means ± SD. *B*: permeability of human-engineered microvessel (hEMV) where collagen channels were coated with recombinant IgG1, rJAG1, or rDLL4 before EC seeding. Representative images of the leak of 70 kDa dextran dye through hEMV at 0 and 105 s (*left*) and quantification of the coefficient of diffusive permeability of 70 kDa dextran (*right*). Scale bars 50 μm. Whiskers calculated using Tukey's method. *C*: Western blot for DLL4 and JAG1 in Scr and N3^{KO} pericytes cultured on rIgG1- or rJAG1-coated plates for 24 h (*top*), and quantification relative to loading control (*bottom*). Means ± SD. *D*: schematic of the proposed mechanism. In pericytes (green), NOTCH3 is activated by JAG1, stimulating an increase in DLL4 expression. DLL4 binds NOTCH1 in adjacent endothelial cells (pink), activating NOTCH1 and stabilizing junctions. For *A* and *B*, *P* values calculated using ordinary one-way ANOVA with multiple comparisons. For *C*, *P* values calculated using two-way ANOVA with multiple comparisons. *$P < 0.05$, **$P < 0.01$, ***$P < 0.001$, ****$P < 0.0001$.

Pericyte Expression of DLL4 Is Enhanced by NOTCH3-JAG1 Interaction

Thus far, our data suggest a need for both EC NOTCH1 and PC NOTCH3 for microvessels to form stable junctions. In addition, we had observed that DLL4 was a key ligand that could stimulate NOTCH1 activation and junctional stabilization in endothelial cells. Together, these data suggested the possibility that DLL4 expression in pericytes could be dependent on NOTCH3 transcription. It has been shown that mural cells interact with the endothelium by binding endothelial JAG1 (30, 32, 40), so we plated the Scr and N3^{KO} pericytes on either IgG1- or rJAG1-coated substrates and assessed the levels of DLL4 and JAG1 protein in these cells after 24 h (Fig. 5*C*). In the control condition, there was no difference in the baseline level of DLL4 or JAG1 expressed by the Scr or N3^{KO} pericytes. However, interaction with JAG1 increased the expression of DLL4 in Scr PCs twofold relative to PCs plated on IgG1 and this increase was absent in N3^{KO} pericytes (Fig. 5*C*). JAG1 expression did not vary significantly in PCs plated on rJAG1. To test whether the upregulation of DLL4 upon activation of NOTCH3 was a general mural cell property, we repeated this experiment with human aortic smooth muscle cells (hASMCs). These hASMCs did not increase DLL4 expression upon plating on JAG1 and generally expressed less NOTCH3 protein than the PCs (Supplemental Fig. S5*B*), suggesting a PC-specific behavior. Based on these data, we propose that interaction of NOTCH3-JAG1 stimulates DLL4 upregulation in pericytes and this DLL4 contributes to the activation of endothelial NOTCH1, thus stabilizing the vascular barrier (Fig. 5*D*).

DISCUSSION

Here, we show that both pericyte NOTCH3 and endothelial NOTCH1 are required to stabilize endothelial cell junctions, that DLL4 activates NOTCH1 to stimulate vascular barrier, and that the interaction of NOTCH3 with JAG1 increases DLL4 in pericytes. Therefore, we suggest a

complex handshake between endothelial cells and pericytes that supports vascular stability. Endothelial cells express JAG1 ligand, which activates NOTCH3 on pericytes, and thus stimulates DLL4 upregulation in pericytes. This DLL4 then activates NOTCH1 on the endothelial cells and promotes vascular junction stabilization. This study sheds light on the interplay between different Notch receptors in the vasculature and suggests interconnection between the NOTCH1 and NOTCH3 pathways. Prior work has shown that deficiency of NOTCH1 and NOTCH3 has combinatorial effects on in vivo vasculature development, disrupting plexus density, basement membrane integration, and pericyte coverage (41); however, this study did not look in-depth at endothelial adherens junctions. Our results suggest complementary roles for NOTCH1 and NOTCH3 in the maintenance of endothelial cell-cell junctions. Our study did not observe the same dramatic alteration of the vascular network structure and pericyte coverage, but this could be due to a context-dependent difference between our in vitro systems compared with the in vivo mouse studies.

The vascular effects of NOTCH3 mutations in pericytes remain inconclusive due to conflicting reports (18, 20), although Notch transcription within pericytes has been shown to be key for the maintenance of endothelial junctions (42). Our results suggest that NOTCH3 specifically contributes to pericyte-induced stabilization of vascular junctions. NOTCH3^{KO} pericytes did not stabilize the barrier or recruit p120-catenin and VE-cadherin to endothelial adherens junctions to the same extent as control pericytes. These findings could relate to the vascular pathologies reported in CADASIL, a disease where aberrant NOTCH3 signaling may impact disease phenotype (43). Perhaps the cross talk with endothelial NOTCH1 signaling in our study also plays a role in such disease settings. In addition, pericytes may play a key role in inflammatory conditions (44) and Alzheimer's disease (45), but it is not yet clear whether there is a role for NOTCH1-NOTCH3 cross talk in these situations. Despite the importance of NOTCH3 in this work, we observed that the NOTCH3^{KO} pericytes were still able to partially support vascular stabilization compared with vessels formed without pericytes. This partial effect could be explained by the NOTCH3^{KO} pericyte maintenance of a basal, NOTCH3-independent, level of DLL4 expression that is sufficient to partially stimulate endothelial junctions. It is also possible that NOTCH3^{KO} pericytes continue to impact endothelial cells through alternate mechanisms. For instance, pericytes have previously been shown to interact with endothelial cells through Ang1 (14, 15), PDGFR-β (11–13), TGF-β (46–48), gap junctions (47–50), and N-cadherin engagement (39, 46, 51–53) among other mechanisms (17). Here, we suggest that Notch signaling between pericytes and endothelial cells adds to the complex interaction of these two cell types.

In addition to pericytes, vascular smooth muscle cells (VSMCs) have been reported to regulate vascular permeability (54). Despite the importance of NOTCH3-JAG1 interactions on VSMC differentiation and localization (19, 20, 30, 31), we did not observe an increase in DLL4 expression in VSMCs plated on rJAG1, suggesting that this mechanism may be primarily at play within capillaries. Interestingly, high levels of shear robustly activate NOTCH1 as a direct mechanism to support barrier function in arteries (8), whereas in capillaries, shear is typically more intermittent. Taken together, it is tempting to speculate that presentation of DLL4 by pericytes may act to stabilize endothelial junctions to compensate for the intermittent shear in small vessels. Future efforts to investigate hierarchy-specific vascular models will shed light on the balance of NOTCH1 activation by shear or mural cells through the vascular system.

There is still much to learn about how Notch drives different tissue functions, but recent work has begun to uncover cross talk between different Notch receptors. A study by Ohashi et al. (55) demonstrated NOTCH1-stimulated *NOTCH3* gene expression, which together coordinated to regulate esophageal squamous differentiation. Complex interaction of multiple Notch signaling components has also been shown to impact macrophage phenotype and it has been hypothesized that feedback loops between Notch signaling and inflammatory signaling may help promote and sustain macrophage activation (56). One study demonstrated that differentiation of monocytes to macrophages triggered an upregulation of NOTCH3 and stimulation of these macrophages with LPS increased DLL4 and *JAG1* expression. Furthermore, macrophage interaction with rDLL4-activated NOTCH1 and upregulated proinflammatory genes, suggesting interplay between Notch signaling and inflammation in macrophages (57). Notch signaling cross talk between two different cell types have been reported by Delgado-Calle et al. (58), where the interaction of osteocytes with multiple myeloma (MM) cells promoted NOTCH3 expression and activation, and stimulation by DLL1 triggered osteocyte apoptosis. Meanwhile, osteocytes-activated Notch in MM cells to stimulate *NOTCH3* and *NOTCH4* expression and enhance MM proliferation, suggesting a role for reciprocal Notch signaling on multiple myeloma progression (58). Here, we add another example of Notch cross talk to coordinate two different cell types in a vascular-specific context. Given the central role of both Notch signaling and heterotypic cell-cell interactions in many tissue contexts, we anticipate that Notch cross talk will emerge as a widely used mechanism to coordinate bidirectional cell-cell interactions.

SUPPLEMENTAL DATA

Supplemental Tables S1 and S2 and Supplemental Figs. S1-S5: https://doi.org/10.6084/m9.figshare.16499511.v1.

Supplemental Movie 1: https://doi.org/10.6084/m9.figshare.16499517.v1.

Supplemental Movie 2: https://doi.org/10.6084/m9.figshare.16499547.v1.

GRANTS

This work was supported by the National Institutes of Health Grants EB000262, EB008396, and HL147585 and by the US-Israel Binational Science Foundation (2017239). J.B.T. acknowledges support from the NIH through the Translational Research in Biomaterials Training Program (No. T32 EB006359). J.L.B. acknowledges support from the NIH National Research Service Awards T32 EB16652 and F32 HL154664. A.L. acknowledges support from the NIH T32 Quantitative Biology and Physiology training grant and from the National Institute of Health NHLBI (No. F31 HL156517).

DISCLOSURES

No conflicts of interest, financial or otherwise, are declared by the authors.

AUTHOR CONTRIBUTIONS

J.B.T., A.L., S.K., and C.S.C. conceived and designed research; J.B.T., J.L.B., and A.L. performed experiments; J.B.T., J.L.B., and A.L. analyzed data; J.B.T. and C.S.C. interpreted results of experiments; J.B.T. prepared figures; J.B.T. drafted manuscript; J.B.T., J.L.B., S.K., J.E., and C.S.C. edited and revised manuscript; J.B.T., J.L.B., A.L., S.K., J.E., and C.S.C. approved final version of manuscript.

REFERENCES

1. **Gazave E**, **Lapébie P**, **Richards GS**, **Brunet F**, **Ereskovsky AV**, **Degnan BM**, **Borchiellini C**, **Vervoort M**, **Renard E.** Origin and evolution of the Notch signalling pathway: an overview from eukaryotic genomes. *BMC Evol Biol* 9: 249, 2009. doi:10.1186/1471-2148-9-249.
2. **Artavanis-Tsakonas S**, **Rand MD**, **Lake RJ.** Notch signaling: cell fate control and signal integration in development. *Science* 284: 770–776, 1999. doi:10.1126/science.284.5415.770.
3. **Bray SJ.** Notch signalling in context. *Nat Rev Mol Cell Biol* 17: 722–735, 2016. doi:10.1038/nrm.2016.94.
4. **Lai EC.** Notch signaling: control of cell communication and cell fate. *Development* 131: 965–973, 2004. doi:10.1242/dev.01074.
5. **Phng LK**, **Gerhardt H.** Angiogenesis: a team effort coordinated by Notch. *Dev Cell* 16: 196–208, 2009. doi:10.1016/j.devcel.2009.01.015.
6. **Hellström M**, **Phng LK**, **Hofmann JJ**, **Wallgard E**, **Coultas L**, **Lindblom P**, **Alva J**, **Nilsson AK**, **Karlsson L**, **Gaiano N**, **Yoon K**, **Rossant J**, **Iruela-Arispe ML**, **Kalén M**, **Gerhardt H**, **Betsholtz C.** Dll4 signalling through Notch1 regulates formation of tip cells during angiogenesis. *Nature* 445: 776–780, 2007. doi:10.1038/nature05571.
7. **Polacheck WJ**, **Kutys ML**, **Yang J**, **Eyckmans J**, **Wu Y**, **Vasavada H**, **Hirschi KK**, **Chen CS.** A non-canonical Notch complex regulates adherens junctions and vascular barrier function. *Nature* 552: 258–262, 2017. doi:10.1038/nature24998.
8. **Mack JJ**, **Mosqueiro TS**, **Archer BJ**, **Jones WM**, **Sunshine H**, **Faas GC**, **Briot A**, **Aragón RL**, **Su T**, **Romay MC**, **McDonald AI**, **Kuo C-H**, **Lizama CO**, **Lane TF**, **Zovein AC**, **Fang Y**, **Tarling EJ**, **de Aguiar Vallim TQ**, **Navab M**, **Fogelman AM**, **Bouchard LS**, **Iruela-Arispe ML**, **Iruela-Arispe ML.** NOTCH1 is a mechanosensor in adult arteries. *Nat Commun* 8: 1620, 2017. doi:10.1038/s41467-017-01741-8.
9. **Fang JS**, **Coon BG**, **Gillis N**, **Chen Z**, **Qiu J**, **Chittenden TW**, **Burt JM**, **Schwartz MA**, **Hirschi KK.** Shear-induced Notch-Cx37-p27 axis arrests endothelial cell cycle to enable arterial specification. *Nat Commun* 8: 2149, 2017. doi:10.1038/s41467-017-01742-7.
10. **Winkler EA**, **Bell RD**, **Zlokovic BV.** Central nervous system pericytes in health and disease. *Nat Neurosci* 14: 1398–1405, 2011. doi:10.1038/nn.2946.
11. **Armulik A**, **Genové G**, **Mäe M**, **Nisancioglu MH**, **Wallgard E**, **Niaudet C**, **He L**, **Norlin J**, **Lindblom P**, **Strittmatter K**, **Johansson BR**, **Betsholtz C.** Pericytes regulate the blood-brain barrier. *Nature* 468: 557–561, 2010. doi:10.1038/nature09522.
12. **Daneman R**, **Zhou L**, **Kebede AA**, **Barres BA.** Pericytes are required for blood-brain barrier integrity during embryogenesis. *Nature* 468: 562–566, 2010. doi:10.1038/nature09513.
13. **Bell RD**, **Winkler EA**, **Sagare AP**, **Singh I**, **LaRue B**, **Deane R**, **Zlokovic BV.** Pericytes control key neurovascular functions and neuronal phenotype in the adult brain and during brain aging. *Neuron* 68: 409–427, 2010. doi:10.1016/j.neuron.2010.09.043.
14. **Thurston G**, **Suri C**, **Smith K**, **McClain J**, **Sato TN**, **Yancopoulos GD**, **McDonald DM.** Leakage-resistant blood vessels in mice transgenically overexpressing angiopoietin-1. *Science* 286: 2511–2514, 1999. doi:10.1126/science.286.5449.2511.
15. **Maisonpierre PC**, **Suri C**, **Jones PF**, **Bartunkova S**, **Wiegand SJ**, **Radziejewski C**, **Compton D**, **McClain J**, **Aldrich TH**, **Papadopoulos N**, **Daly TJ**, **Davis S**, **Sato TN**, **Yancopoulos GD.** Angiopoietin-2, a natural antagonist for Tie2 that disrupts in vivo angiogenesis. *Science* 277: 55–60, 1997. doi:10.1126/science.277.5322.55.
16. **Gaengel K**, **Genové G**, **Armulik A**, **Betsholtz C.** Endothelial-mural cell signaling in vascular development and angiogenesis. *Arterioscler Thromb Vasc Biol* 29: 630–638, 2009. doi:10.1161/ATVBAHA.107.161521.
17. **Armulik A**, **Genové G**, **Betsholtz C.** Pericytes: developmental, physiological, and pathological perspectives, problems, and promises. *Dev Cell* 21: 193–215, 2011. doi:10.1016/j.devcel.2011.07.001.
18. **Henshall TL**, **Keller A**, **He L**, **Johansson BR**, **Wallgard E**, **Raschperger E**, **Mäe MA**, **Jin S**, **Betsholtz C**, **Lendahl U.** Notch3 is necessary for blood vessel integrity in the central nervous system. *Arterioscler Thromb Vasc Biol* 35: 409–420, 2015. doi:10.1161/ATVBAHA.114.304849.
19. **Domenga V**, **Fardoux P**, **Lacombe P**, **Monet M**, **Maciazek J**, **Krebs LT**, **Klonjkowski B**, **Berrou E**, **Mericskay M**, **Li Z**, **Tournier-Lasserve E**, **Gridley T**, **Joutel A.** Notch3 is required for arterial identity and maturation of vascular smooth muscle cells. *Genes Dev* 18: 2730–2735, 2004. doi:10.1101/gad.308904.
20. **Liu H**, **Zhang W**, **Kennard S**, **Caldwell RB**, **Lilly B.** Notch3 is critical for proper angiogenesis and mural cell investment. *Circ Res* 107: 860–870, 2010. doi:10.1161/CIRCRESAHA.110.218271.
21. **Chabriat H**, **Joutel A**, **Dichgans M**, **Tournier-Lasserve E**, **Bousser M-G.** CADASIL. *Lancet Neurol* 8: 643–653, 2009. doi:10.1016/S1474-4422(09)70127-9.
22. **Schmidt H**, **Zeginigg M**, **Wiltgen M**, **Freudenberger P**, **Petrovic K**, **Cavalieri M**, **Gider P**, **Enzinger C**, **Fornage M**, **Debette S**, **Rotter JI**, **Ikram MA**, **Launer LJ**, **Schmidt R**; **CHARGE consortium Neurology working group.** Genetic variants of the NOTCH3 gene in the elderly and magnetic resonance imaging correlates of age-related cerebral small vessel disease. *Brain* 134: 3384–3397, 2011. doi:10.1093/brain/awr252.
23. **Ter Telgte A**, **van Leijsen EMC**, **Wiegertjes K**, **Klijn CJM**, **Tuladhar AM**, **De Leeuw FE.** Cerebral small vessel disease: from a focal to a global perspective. *Nat Rev Neurol* 14: 387–398, 2018. doi:10.1038/s41582-018-0014-y.
24. **Concordet JP**, **Haeussler M.** CRISPOR: intuitive guide selection for CRISPR/Cas9 genome editing experiments and screens. *Nucleic Acids Res* 46: W242–W245, 2018. doi:10.1093/nar/gky354.
25. **Kim S**, **Lee H**, **Chung M**, **Jeon NL.** Engineering of functional, perfusable 3D microvascular networks on a chip. *Lab Chip* 13: 1489–1500, 2013. [Erratum in *Lab Chip* 13: 4891, 2013]. doi:10.1039/c3lc41320a.
26. **Schneider CA**, **Rasband WS**, **Eliceiri KW.** NIH Image to ImageJ: 25 years of image analysis. *Nat Methods* 9: 671–675, 2012. doi:10.1038/nmeth.2089.
27. **Polacheck WJ**, **Kutys ML**, **Tefft JB**, **Chen CS.** Microfabricated blood vessels for modeling the vascular transport barrier. *Nat Protoc* 14: 1425–1454, 2019. doi:10.1038/s41596-019-0144-8.
28. **Campisi M**, **Shin Y**, **Osaki T**, **Hajal C**, **Chiono V**, **Kamm RD.** 3D self-organized microvascular model of the human blood-brain barrier with endothelial cells, pericytes and astrocytes. *Biomaterials* 180: 117–129, 2018. doi:10.1016/j.biomaterials.2018.07.014.
29. **Stratman AN**, **Malotte KM**, **Mahan RD**, **Davis MJ**, **Davis GE.** Pericyte recruitment during vasculogenic tube assembly stimulates endothelial basement membrane matrix formation. *Blood* 114: 5091–5101, 2009. doi:10.1182/blood-2009-05-222364.
30. **Liu H**, **Kennard S**, **Lilly B.** NOTCH3 expression is induced in mural cells through an autoregulatory loop that requires endothelial-expressed JAGGED1. *Circ Res* 104: 466–475, 2009. doi:10.1161/CIRCRESAHA.108.184846.
31. **Edwards AK**, **Glithero K**, **Grzesik P**, **Kitajewski AA**, **Munabi NCO**, **Hardy K**, **Tan QK**, **Schonning M**, **Kangsamaksin T**, **Kitajewski JK**, **Shawber CJ**, **Wu JK.** NOTCH3 regulates stem-to-mural cell differentiation in infantile hemangioma. *JCI Insight* 2: 1–14, 2017. doi:10.1172/jci.insight.93764.
32. **Pedrosa AR**, **Trindade A**, **Fernandes AC**, **Carvalho C**, **Gigante J**, **Tavares AT**, **Diéguez-Hurtado R**, **Yagita H**, **Adams RH**, **Duarte A.** Endothelial jagged1 antagonizes Dll4 regulation of endothelial branching and promotes vascular maturation downstream of Dll4/Notch1. *Arterioscler Thromb Vasc Biol* 35: 1134–1146, 2015. doi:10.1161/ATVBAHA.114.304741.
33. **Giannotta M**, **Trani M**, **Dejana E.** VE-cadherin and endothelial adherens junctions: active guardians of vascular integrity. *Dev Cell* 26: 441–454, 2013. doi:10.1016/j.devcel.2013.08.020.

34. **Grimsley-Myers CM**, **Isaacson RH**, **Cadwell CM**, **Campos J**, **Hernandes MS**, **Myers KR**, **Seo T**, **Giang W**, **Griendling KK**, **Kowalczyk AP.** VE-cadherin endocytosis controls vascular integrity and patterning during development. *J Cell Biol* 219: e201909081, 2020. doi:10.1083/jcb.201909081.
35. **Davis MA**, **Ireton RC**, **Reynolds AB.** A core function for p120-catenin in cadherin turnover. *J Cell Biol* 163: 525–534, 2003. doi:10.1083/jcb.200307111.
36. **Bentley K**, **Franco CA**, **Philippides A**, **Blanco R**, **Dierkes M**, **Gebala V**, **Stanchi F**, **Jones M**, **Aspalter IM**, **Cagna G**, **Weström S**, **Claesson-Welsh L**, **Vestweber D**, **Gerhardt H.** The role of differential VE-cadherin dynamics in cell rearrangement during angiogenesis. *Nat Cell Biol* 16: 309–321, 2014. doi:10.1038/ncb2926.
37. **Barry AK**, **Wang N**, **Leckband DE.** Local VE-cadherin mechanotransduction triggers long-ranged remodeling of endothelial monolayers. *J Cell Sci* 128: 1341–1351, 2015. doi:10.1242/jcs.159954.
38. **Taha AA**, **Taha M**, **Seebach J**, **Schnittler HJ.** ARP2/3-mediated junction-associated lamellipodia control VE-cadherin-based cell junction dynamics and maintain monolayer integrity. *Mol Biol Cell* 25: 245–256, 2014. doi:10.1091/mbc.E13-07-0404.
39. **Alimperti S**, **Mirabella T**, **Bajaj V**, **Polacheck W**, **Pirone DM**, **Duffield J**, **Eyckmans J**, **Assoian RK**, **Chen CS.** Three-dimensional biomimetic vascular model reveals a RhoA, Rac1, and N -cadherin balance in mural cell – endothelial cell-regulated barrier function. *Proc Natl Acad Sci USA* 114: 8758–8763, 2017. doi:10.1073/pnas.1618333114.
40. **High FA**, **Min ML**, **Pear WS**, **Loomes KM**, **Kaestner KH**, **Epstein JA.** Endothelial expression of the Notch ligand Jagged1 is required for vascular smooth muscle development. *Proc Natl Acad Sci U S A* 105: 1955–1959, 2008. doi:10.1073/pnas.0709663105.
41. **Kofler NM**, **Cuervo H**, **Uh MK**, **Murtomäki A**, **Kitajewski J.** Combined deficiency of Notch1 and Notch3 causes pericyte dysfunction, models CADASIL, and results in arteriovenous malformations. *Sci Rep* 5: 16449–16413, 2015. doi:10.1038/srep16449.
42. **Nadeem T**, **Bogue W**, **Bigit B**, **Cuervo H.** Deficiency of Notch signaling in pericytes results in arteriovenous malformations. *JCI Insight* 5: e125940, 2020. doi:10.1172/jci.insight.125940.
43. **Wang MM.** Cadasil. *Handb Clin Neurol* 148: 733–743, 2018. doi:10.1016/B978-0-444-64076-5.00047-8.
44. **Brown LS**, **Foster CG**, **Courtney JM**, **King NE**, **Howells DW**, **Sutherland BA.** Pericytes and neurovascular function in the healthy and diseased brain. *Front Cell Neurosci* 13: 282–289, 2019. doi:10.3389/fncel.2019.00282.
45. **Winkler EA**, **Sagare AP**, **Zlokovic BV.** The pericyte: a forgotten cell type with important implications for alzheimer's disease? *Brain Pathol* 24: 371–386, 2014. doi:10.1111/bpa.12152.
46. **Li F**, **Lan Y**, **Wang Y**, **Wang J**, **Yang G**, **Meng F**, **Han H**, **Meng A**, **Wang Y**, **Yang X.** Endothelial Smad4 Maintains Cerebrovascular Integrity by Activating N-Cadherin through cooperation with Notch. *Dev Cell* 20: 291–302, 2011. doi:10.1016/j.devcel.2011.01.011.
47. **Hirschi KK**, **Burt JM**, **Hirschi KD**, **Dai C.** Gap junction communication mediates transforming growth factor-β activation and endothelial-induced mural cell differentiation. *Circ Res* 93: 429–437, 2003. doi:10.1161/01.RES.0000091259.84556.D5.
48. **Fang JS**, **Dai C**, **Kurjiaka DT**, **Burt JM**, **Hirschi KK.** Connexin45 regulates endothelial-induced mesenchymal cell differentiation toward a mural cell phenotype. *Arterioscler Thromb Vasc Biol* 33: 362–368, 2013. doi:10.1161/ATVBAHA.112.255950.
49. **Ivanova E**, **Kovacs-Oller T**, **Sagdullaev BT.** Vascular pericyte impairment and connexin43 gap junction deficit contribute to vasomotor decline in diabetic retinopathy. *J Neurosci* 37: 7580–7594, 2017. doi:10.1523/JNEUROSCI.0187-17.2017.
50. **Li AF**, **Sato T**, **Haimovici R**, **Okamoto T**, **Roy S.** High glucose alters connexin 43 expression and gap junction intercellular communication activity in retinal pericytes. *Invest Ophthalmol Vis Sci* 44: 5376–5382, 2003. doi:10.1167/iovs.03-0360.
51. **Gerhardt H**, **Wolburg H**, **Redies C.** N-cadherin mediates pericytic-endothelial interaction during brain angiogenesis in the chicken. *Dev Dyn* 218: 472–479, 2000. doi:10.1002/1097-0177(200007)218:3<472::AID-DVDY1008>3.0.CO;2-#.
52. **Paik JH**, **Skoura A**, **Chae SS**, **Cowan AE**, **Han DK**, **Proia RL**, **Hla T.** Sphingosine 1-phosphate receptor regulation of N-cadherin mediates vascular stabilization. *Genes Dev* 18: 2392–2403, 2004. doi:10.1101/gad.1227804.
53. **Kruse K**, **Lee QS**, **Sun Y**, **Klomp J**, **Yang X**, **Huang F**, **Sun MY**, **Zhao S**, **Hong Z**, **Vogel SM**, **Shin JW**, **Leckband DE**, **Tai LM**, **Malik AB**, **Komarova YA.** N-cadherin signaling via Trio assembles adherens junctions to restrict endothelial permeability. *Dev Dyn* 218: 1–28, 2018. doi:10.1083/jcb.201802076.
54. **Zheng B**, **Yin W. N**, **Suzuki T**, **Zhang X-H.**, **Zhang Y**, **Song L. L**, **Jin L. S**, **Zhan H**, **Zhang H**, **Li J. S**, **Wen J. K.** Exosome-Mediated miR-155 Transfer from Smooth Muscle Cells to Endothelial Cells Induces Endothelial Injury and Promotes Atherosclerosis. *Mol Ther* 25: 1279–1294, 2017. doi:10.1016/j.ymthe.2017.03.031.
55. **Ohashi S**, **Natsuizaka M**, **Yashiro-Ohtani Y**, **Kalman RA**, **Nakagawa M**, **Wu L**, **Klein-Szanto AJ**, **Herlyn M**, **Diehl JA**, **Katz JP**, **Pear WS**, **Seykora JT**, **Nakagawa H.** NOTCH1 and NOTCH3 coordinate esophageal squamous differentiation through a csl-dependent transcriptional network. *Gastroenterology* 139: 2113–2123, 2010. doi:10.1053/j.gastro.2010.08.040.
56. **Keewan E**, **Naser SA.** The role of Notch signaling in macrophages during inflammation and infection: implication in rheumatoid arthritis? *Cells* 9: 111, 2020. doi:10.3390/cells9010111.
57. **Fung E**, **Tang SMT**, **Canner JP**, **Morishige K**, **Arboleda-Velasquez JF**, **Cardoso AA**, **Carlesso N**, **Aster JC**, **Aikawa M.** Delta-like 4 induces Notch signaling in macrophages: implications for inflammation. *Circulation* 115: 2948–2956, 2007. doi:10.1161/CIRCULATIONAHA.106.675462.
58. **Delgado-Calle J**, **Anderson J**, **Cregor MD**, **Hiasa M**, **Chirgwin JM**, **Carlesso N**, **Yoneda T**, **Mohammad KS**, **Plotkin LI**, **Roodman GD**, **Bellido T.** Bidirectional notch signaling and osteocyte-derived factors in the bone marrow microenvironment promote tumor cell proliferation and bone destruction in multiple myeloma. *Cancer Res* 76: 1089–1100, 2016. doi:10.1158/0008-5472.CAN-15-1703.